processes

MDPI

Article

Investigation of the Acid Generation Pattern and Flow-Reaction Behavior of Solid Retarded Acid

Jianye Mou [2,*], Jia Cui [1], Kai Chen [1], Lufeng Zhang [1], Xiaowei Li [2], Yunhui Zhang [2] and Budong Gao [2]

[1] Key Laboratory of Marine Oil & Gas Reservoirs Production, Sinopec, Petroleum Exploration and Production Research Institute, Beijing 100083, China; chenkai.syky@sinopec.com (K.C.); zlfcupb@163.com (L.Z.)
[2] College of Petroleum Engineering, China University of Petroleum (Beijing), Beijing 102249, China; cupblxw@163.com (X.L.); gaobd0723@163.com (B.G.)
* Correspondence: moujianye@cup.edu.cn

Abstract

The carbonate reservoir of the Shunbei oilfield is characterized by deep burial depth and high temperature. During acid fracturing, the reaction rate between conventional acid systems and the rock is relatively fast, leading to a limited effective acid penetration distance. To extend the acid penetration distance, a combination of solid retarded acid and conventional acid was used in field operations. The effectiveness of the solid retarded acid depends on its acid generation pattern, making it necessary to study the acid generation behavior of the solid retarded acid. This paper establishes a frame for evaluating the solid retarded acid, including tests for solid retarded acid solubility, acid concentration, and acid-etched fracture conductivity. Based on the test results, the acid generation pattern of solid retarded acid was analyzed, its slow-generation performance was evaluated, and an acid generation model was established. Finally, by integrating the acid generation model with the existing acid fracturing model, the effective distance of solid retarded acid was predicted. The study shows that the solubility of acid-generating materials is influenced by both temperature and solid retarded acid concentration. When the concentration of solid retarded acid exceeds 25%, it does not completely dissolve at room temperature, but can fully dissolve after 40 min at 120 °C. The acid concentration is significantly affected by temperature, with an acid concentration of about 1.6 mol/L at room temperature and up to 3.1 mol/L at high temperatures, comparable to a 12% hydrochloric acid concentration. Solid retarded acid exhibits good slow-generation performance, with a comprehensive reaction rate approximately one-third of that of cross-linked acid. When the acid-rock contact time is around 3 h, the acid-etched fracture conductivity of solid retarded acid can remain above 5 D·cm under a closure pressure of 60 MPa. The predicted effective acid penetration distance of solid retarded acid can reach over 150 m, under typical conditions of Shunbei oilfield. The findings of this study can serve as a reference for the design and optimization of solid retarded acid fracturing.

Keywords: solid retarded acid; solubility; acid generation pattern; slow-generation performance; fracture conductivity; acid penetration distance

Check for updates

Academic Editor: Qiang Yu

Received: 18 November 2025
Revised: 13 December 2025
Accepted: 25 December 2025
Published: 29 December 2025

Copyright: © 2025 by the authors. Licensee MDPI, Basel, Switzerland. This article is an open access article distributed under the terms and conditions of the Creative Commons Attribution (CC BY) license.

1. Introduction

Acid fracturing is a widely applied stimulation technique for carbonate reservoirs [1,2]. The process involves non-uniform etching of fracture surfaces by acid fluids so that, after closure, a residual fracture aperture remains, providing high conductivity. The performance

of acid fracturing is influenced by various parameters. Among these, the acid system is a decisive factor, as it determines the effective acidizing distance, etched fracture morphology, and fracture conductivity [1,3,4].

Recent research has focused on reducing the acid–rock reaction rate and extending the effective penetration distance of the acid. Most studies have achieved retardation by decreasing the hydrogen-ion release rate or its mass-transfer rate [5]. Such systems are collectively known as retarded acids. Currently, commonly used retarded acids include gelled acid, cross-linked acid, self-diverting acid, organic acid, emulsified acid, and authigenic acid [6–9]. Zhang et al. [10] applied organic retarded acid for deep formation treatment, which achieved effective deep acidizing. Field applications in the eastern periphery of the Daqing Oilfield demonstrated promising initial results. Li et al. [11] prepared an emulsifier (CT1-36) based on unsaturated ester and sorbitan oleate. The emulsified acid formulated with this agent maintained a viscosity of 40 mPa·s at 140 °C and 170 s^{-1} for 60 min, with an acid–rock reaction rate one-twentieth that of conventional acid. Nars-El-Din et al. [12] designed an authigenic acid by reacting AlCl3 with HF to generate HCl, effectively slowing the acid–rock reaction. Zhou et al. [13] synthesized a latent acid system using paraformaldehyde, ammonium chloride, xanthan gum, and water. The acid concentration increases with increasing temperature, extending the reaction time to 100 min. At 120 °C, the authigenic acid exhibited stronger etching ability than 20% HCl. These studies demonstrate that controlling acid viscosity, concentration, filtration, hydrogen ions (H^+) mass transfer rate, acid–rock contact area, and hydrogen-ion generation mechanisms can effectively reduce reaction rates and increase acid penetration effective distance.

Although current retarded acids mitigate several issues associated with conventional hydrochloric acid, the issues of excessively rapid acid-rock reaction rates and short effective acid penetration distance persist under ultra-deep and ultra-high-temperature reservoir conditions [14,15]. During acid fracture stimulation of ultra-deep, high-temperature carbonate reservoirs in the Shunbei Oilfield, the reaction rate between conventional acid and rock is particularly sensitive to temperature. The acid solution loses its reactivity before reaching the end of fractures, resulting in a short effective acid penetration distance [16,17]. Emulsified acids exhibit high friction in deep wells, leading to excessive injection pressure and poor operational efficiency [18]. Solid retarded acid, also known as solid retarded acid, represents a type of autogenic acid-generating system. It is produced by solidifying acid-generating materials, crushing them into particles of desired size, and coating them with inert, soluble, or semi-permeable films. During fracturing, the formation is first hydraulically fractured with a pad fluid. Subsequently, solid retarded acid particles are injected into the fractures with a carrier fluid. In the wellbore and during the initial injection stage, the particles remain largely inert or mildly corrosive, not corroding ground equipment. After pumping stops, the particles either settle or suspend within the fractures. Under reservoir conditions, the solid retarded acid gradually hydrolyzes, continuously generating acid and releasing H^+ to dissolve carbonate rock.

Unlike conventional retarded acid systems, the solid retarded acid investigated in this study introduces a novel approach utilizing pulverized, surface-coated organic ester particles. It achieves effective retardation through a controlled multi-stage pathway involving particle injection, thermally induced dissolution, and gradual hydrolysis to release H^+. This solid-to-liquid phase transition mechanism overcomes the limitations of emulsified acids, which exhibit high friction in ultra-deep wells, and traditional autogenic acids, which often react prematurely due to high temperature sensitivity. By pumping solid particles in a neutral carrier fluid, this system significantly reduces friction and surface equipment corrosion. Furthermore, compared to liquid organic acids and cross-linked acids—which typically suffer from filtration loss or rapid concentration decline—the solid retarded acid

maintains a high acid concentration over a prolonged duration. This sustained reactivity enables significant etching even at the fracture tip, effectively extending the acid penetration distance to over 150 m, thereby offering a superior solution for stimulating ultra-deep, high-temperature carbonate reservoirs.

Through simultaneous dissolution and hydrolysis, the solid retarded acid maintains an effective acid concentration for an extended period. This enables sustained and non-uniform etching of the fracture walls, achieving retarded and deep acidizing. Therefore, the system has significant potential for application in ultra-deep, high-temperature carbonate reservoirs. In terms of operations, the friction of solid particles migrating in deep wells is lower than that of liquid acids. Economically, although the material cost is higher than that of HCl, the reduction in corrosion and the production enhancement resulting from deep penetration make the overall cost reasonable. Environmentally, the hydrolysis products primarily consist of organic acids (acetic/lactic acid) and alcohols. These compounds are biodegradable and pose significantly less environmental hazard compared to spent strong mineral acids or flowback fluids containing heavy metal corrosion products. However, limited research has been reported on its acid-generation behavior and acid-rock reaction capacity. In this study, the solubility, acid-generation patterns, and retardation characteristics of the solid retarded acid were investigated experimentally. The solubility of the acid-generating material was first measured. Acid concentration as a function of temperature and time was determined using acid–base titration, and a mathematical model of acid-generation concentration was established. Subsequently, acid–rock reaction tests using carbonate slabs were conducted to assess the etching capacity and reaction rate. The etching capability of the solid retarded acid was compared with that of gelled and cross-linked acids to evaluate its retardation performance. The acid-etched rock slabs are then tested to evaluate the fracture conductivity generated by solid retarded acid. A comprehensive evaluation method for solid retarded acid performance was thus developed. Finally, by integrating the acid-generation model with an acid-fracturing model, the effective acid penetration distance was predicted.

2. Dissolution Behavior of Solid Retarded Acid

During acid fracturing, solid retarded acid is introduced into the fracture as solid particles carried by a neutral carrier fluid. Within the fracture, the particles dissolve progressively as the temperature increases and hydrolyze to generate acid. The dissolution behavior of the solid retarded acid-generating material varies with temperature, concentration, and time. To ensure that the solid retarded acid particles in the carrier fluid can completely dissolve under reservoir conditions while generating sufficient acid concentration, solubility tests of the solid retarded acid particles were first conducted.

2.1. Experimental Materials and Methods

The solid retarded acid used in this study was an organic ester-based retarded acid developed by Sinopec Northwest Branch. It was formulated by blending polyvinyl acetate, polylactate ester, methyl formate, and other ester compounds in specific proportions. The carrier fluid was a high-viscosity fracturing fluid thickened with 0.7% gelling agent supplied by Dongying Spring Petroleum Engineering Technology, China. To investigate the effects of temperature, concentration, and time on the dissolution behavior of the solid retarded acid, mixtures of solid retarded acid and carrier fluid were prepared at mass concentrations of 20%, 25%, 30%, and 40%. Each mixture was stirred for 10 min and then transferred into a Hastelloy high-pressure vessel that had been preheated in an oven. Nitrogen gas was introduced to the vessel to raise the internal pressure to 1.5 atm, ensuring that the maximum solution temperature could reach 120 °C. The oven temperature was

then adjusted according to the experimental plan. At the specified test time, the vessel pressure was released, and the mixture was removed for analysis. The undissolved solids were separated by filtration, dried in an oven, and weighed. The dissolution ratio of the solid retarded acid material was calculated as the ratio of the remaining solid mass to the initial solid mass. The detailed experimental scheme is shown in Table 1.

Table 1. Experimental scheme for the dissolution rate of solid retarded acids.

Mixture Number	Solid Retarded Acid Concentration	Temperature (°C)	Time (min)
0#	20	25	0
1#–7# 8#–14	25	25 120	0, 20, 40, 60, 80, 100, 120
15#–21# 22#–28# 29#–35#	30	25 90 120	0, 20, 40, 60, 80, 100, 120
36#–42# 43#–49# 50#–56#	40	25 90 120	0, 20, 40, 60, 80, 100, 120

2.2. Experimental Results and Analysis

The dissolution behavior of solid retarded acid with acid-generating material concentrations of 20% and 30% at room temperature, 90 °C, and 120 °C is shown in Figure 1. As the temperature increased, the color of the solid retarded acid mixtures gradually became lighter, and the amount of undissolved material decreased. Similar phenomena were observed for other concentrations. This occurred because, after dissolution, the solid retarded acid hydrolyzed to produce organic acids and alcohols. Since the hydrolysis products are transparent liquids, the overall color of the solution became lighter. With increasing temperature, the degree of hydrolysis increased, leading to higher concentrations of organic acids and further color fading.

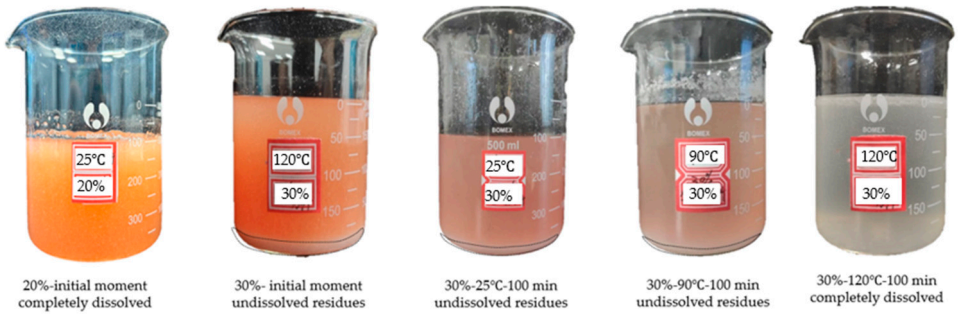


Figure 1. Effect of temperature on the dissolution of solid retarded acid: High temperature significantly promotes solution clarification and complete dissolution.

The dissolution rates of the solid retarded acid-generating materials at various concentrations, temperatures, and times were measured. Experiments for each concentration were conducted in triplicate, and the average values were calculated, as presented in Table 2a–c.

Table 2. (**a**) Dissolution rate of acid-generating material at 25% concentration. (**b**) Dissolution rate of acid-generating material at 30% concentration. (**c**) Dissolution rate of acid-generating material at 40% concentration.

(a)

Time (min)	Temperature (°C)	Group 1 Dissolution Rate (%)	Group 2 Dissolution Rate (%)	Group 3 Dissolution Rate (%)	Mean Dissolution Rate (%)
0	25 °C	78.47	79.28	82.55	80.1
20	25 °C	87.73	83.25	84.62	85.2
40	25 °C	88.05	88.94	85.51	87.5
60	25 °C	89.26	89.27	91.77	90.1
80	25 °C	88.89	90.49	91.22	90.2
100	25 °C	89.92	91.31	89.22	90.15
120	25 °C	88.93	90.96	90.86	90.25
0	120 °C	78.36	82.7	79.84	80.3
20	120 °C	100	100	100	100
40	120 °C	100	100	100	100
60	120 °C	100	100	100	100
80	120 °C	100	100	100	100
100	120 °C	100	100	100	100
120	120 °C	100	100	100	100

(b)

Time (min)	Temperature (°C)	Group 1 Dissolution Rate (%)	Group 2 Dissolution Rate (%)	Group 3 Dissolution Rate (%)	Mean Dissolution Rate (%)
0	25 °C	64.15	61.6	60.55	62.1
20	25 °C	63.76	61.28	65.46	63.5
40	25 °C	62.97	66.07	66.57	65.2
60	25 °C	69.01	65.96	70.23	68.4
80	25 °C	69.22	68.68	71.5	69.8
100	25 °C	69.83	69.08	71.39	70.1
120	25 °C	68.86	70.52	71.07	70.15
0	90 °C	61.85	64.39	60.66	62.3
20	90 °C	68.46	73.28	69.76	70.5
40	90 °C	77.29	76.28	72.03	75.2
60	90 °C	85.39	81.91	86.5	84.6
80	90 °C	91.59	87.48	90.33	89.8
100	90 °C	96.14	98.42	97.94	97.5
120	90 °C	99.78	100.11	99.51	99.8
0	120 °C	61.34	64.75	61.11	62.4
20	120 °C	88.03	92.93	87.54	89.5
40	120 °C	99.73	100.02	99.95	99.9
60	120 °C	100	100	100	100
80	120 °C	100	100	100	100
100	120 °C	100	100	100	100
120	120 °C	100	100	100	100

(c)

Time (min)	Temperature (°C)	Group 1 Dissolution Rate (%)	Group 2 Dissolution Rate (%)	Group 3 Dissolution Rate (%)	Mean Dissolution Rate (%)
0	25 °C	47.93	52.88	49.79	50.2
20	25 °C	50.31	55.26	50.73	52.1
40	25 °C	55.33	52.83	58.04	55.4
60	25 °C	57.38	60.91	56.31	58.2
80	25 °C	61.64	58.01	60.65	60.1
100	25 °C	61.27	58.46	60.72	60.15
120	25 °C	61.25	60.77	58.58	60.2
0	90 °C	47.58	52.74	50.88	50.4
20	90 °C	57.38	60.54	63.58	60.5
40	90 °C	66.86	73.25	70.49	70.2
60	90 °C	77.29	80.12	82.89	80.1
80	90 °C	89.14	88.19	92.37	89.9
100	90 °C	96.47	98.13	98.8	97.8
120	90 °C	100	100	100	100
0	120 °C	53.07	47.97	50.46	50.5
20	120 °C	72.39	79.11	74.1	75.2
40	120 °C	100	100	100	100
60	120 °C	100	100	100	100
80	120 °C	100	100	100	100
100	120 °C	100	100	100	100
120	120 °C	100	100	100	100

Solid retarded acid dissolution rate curves are presented in Figure 2. When the solid retarded acid concentration was below 20%, the mixture completely dissolved at room temperature after stirring, with a dissolution ratio of 100%. As the concentration of solid retarded acid increased, the initial dissolution ratio decreased. This trend occurred because

solubility is constant at a given temperature; thus, a higher solid content results in a lower apparent dissolution ratio. The dissolution ratio increased with both temperature and time. When the solid retarded acid concentration reached 40%, complete dissolution (100%) was achieved after 40 min at 120 °C. This is attributed to the increase in solubility with temperature. To ensure that the carrier fluid transports the maximum possible concentration of acid-generating material while avoiding excessive undissolved solids that could cause blockage within the fracture, the optimal concentration of the solid retarded acid should be maintained at approximately 30%.

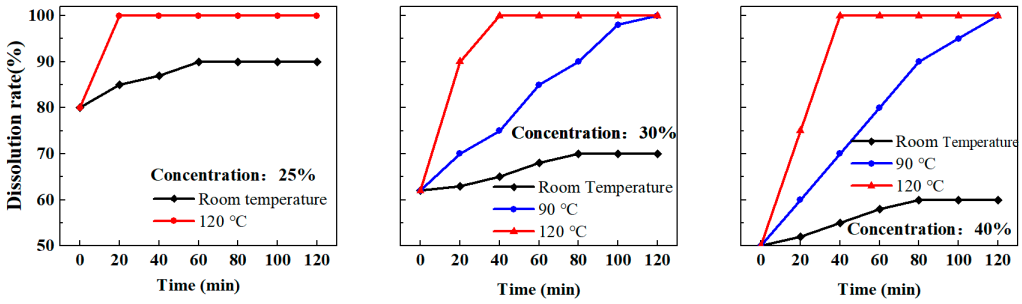


Figure 2. Temperature-dominated material dissolution: Acid-generating materials achieve complete dissolution within 40 min at 120 °C.

3. The Acid Generation Behavior of Solid Retarded Acid

3.1. Principle of Solid Retarded Acid Generation

During the experiment, the solid retarded acid particles gradually dissolved under temperature control, forming a homogeneous solution. In the presence of water molecules, the acyloxy bonds were cleaved through hydrolysis, continuously producing strong organic acids and alcohols. The generated organic acids ionized to release H^+, which reacted with carbonate rock, resulting in dissolution and etching. Since the hydrolysis process that generates H^+ is essentially a reversible chemical reaction, both the reaction rate and equilibrium are highly sensitive to temperature and reactant concentration. Therefore, further experiments were conducted to investigate the acid-generation rules of the solid retarded acid.

3.2. Experimental Methods and Procedures

The acid generation of the solid retarded acid in aqueous solution occurs through a gradual dissolution and release of H^+. The hydrogen ion concentration in the solution was determined via acid-base titration. Specifically, a standard NaOH solution with a precise concentration of 0.1000 mol/L was first prepared and then subjected to secondary standardization using potassium hydrogen phthalate (KHP) as the primary standard to accurately calibrate the solution. This calibration process was performed in triplicate, with the relative standard deviation (RSD) controlled within 0.1% to ensure the accuracy of the standard solution's concentration. Subsequently, for sample titration, a specific volume of the acid sample was aliquoted, mixed with an appropriate amount of indicator (e.g., phenolphthalein), and titrated with the standardized NaOH solution. Finally, the acid concentration was calculated based on the aliquot volume of the acid sample, the recorded volume of NaOH consumed, and the concentration of the standard solution. To investigate the acid generation behaviors, a 30% solid retarded acid solution was prepared and stirred for 10 min to ensure complete dissolution. The prepared solution was then transferred into an oven, where the temperature was set to 25 °C, 90 °C, and 120 °C, respectively. Under each temperature condition, the solution was continuously stirred to promote dissolution and acid generation, following the same preparation procedure

described in Section 2.1. Samples were collected at 20-min intervals. The acid concentration generated at each sampling time was determined by acid–base titration using a sodium hydroxide solution of known concentration [18,19]. Based on the measured data, the acid-generation behavior of the solid retarded acid was analyzed, and a mathematical model describing the acid-generation kinetics was established using regression analysis.

3.3. Experimental Results and Analysis

Acid concentrations at 25 °C, 90 °C, and 120 °C were measured at 20-min intervals over a 2-h period. Measurements were taken in triplicate, and the average concentrations are listed in Table 3.

Table 3. Acid concentration at different temperatures.

Temperature (°C)	Time (min)	Group 1 Acid Concentration (mol/L)	Group 2 Acid Concentration (mol/L)	Group 3 Acid Concentration (mol/L)	Mean Acid Concentration (mol/L)
25	0	1.67	1.62	1.72	1.67
	20	1.69	1.76	1.66	1.70
	40	1.86	1.83	1.77	1.82
	60	1.82	1.79	1.89	1.83
	80	1.88	1.86	1.78	1.84
	100	1.89	1.87	1.79	1.85
	120	1.92	1.85	1.82	1.86
90	0	1.70	1.70	1.61	1.67
	20	2.25	2.30	2.20	2.25
	40	2.51	2.54	2.44	2.50
	60	2.86	2.81	2.76	2.81
	80	2.86	2.77	2.83	2.82
	100	2.74	2.82	2.83	2.80
	120	2.81	2.91	2.83	2.85
120	0	1.62	1.72	1.68	1.67
	20	2.32	2.24	2.34	2.30
	40	3.04	2.98	2.95	2.99
	60	3.08	3.15	3.05	3.09
	80	3.04	2.94	3.02	3.00
	100	3.05	3.15	3.11	3.10
	120	3.06	3.16	3.12	3.11

The acid-generation behavior of the solid retarded acid solution is illustrated in Figure 3. Both the acid concentration and the acid-generation rate increased with temperature. At a constant temperature, the acid concentration gradually rose with the progress of hydrolysis and then tended to stabilize after a certain period. Thereafter, as the reactant concentration decreased, the hydrolysis reaction rate slowed significantly, and the acid concentration entered a phase of slow growth rather than ceasing completely. At the initial stage, the acid concentration was 1.67 mol/L. This initial concentration is attributed to the 10-min stirring process during preparation, which induced partial hydrolysis of the ester materials, resulting in the accumulation of a certain amount of acid. As hydrolysis proceeded, the concentration increased continuously. At room temperature, the acid concentration reached 1.86 mol/L after 120 min and then stabilized. Under a temperature of 90 °C, the acid-generation rate increased significantly, and the stabilized concentration was notably higher than that at room temperature, reaching 2.85 mol/L after 120 min. Under 120 °C, both the acid-generation rate and the equilibrium concentration were the highest, with the acid concentration stabilizing at 3.10 mol/L after 120 min. Overall, a higher temperature resulted in a faster hydrolysis rate, a more rapid increase in acid concentration, and a higher equilibrium acid concentration. This behavior occurs because the hydrolysis of solid retarded acid is an endothermic process, where elevated temperature accelerates the reaction rate and shifts the chemical equilibrium toward the product side, enhancing acid generation.

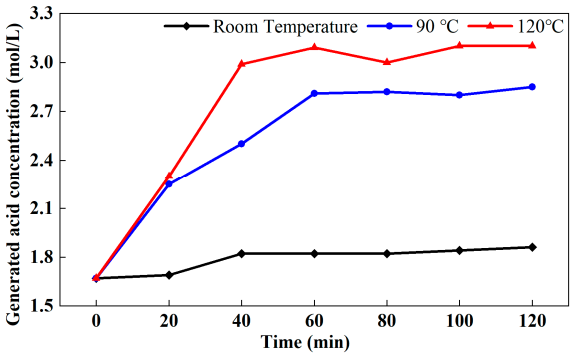


Figure 3. Temperature significantly enhances acid generation capability: Acid concentration reaches 3.1 mol/L and remains stable at 120 °C.

Since the target formation temperature in the Shunbei Oilfield exceeds 120 °C, determining the long-term acid generation performance at this specific temperature is critical for evaluating the acid's effectiveness. Therefore, an extended hydrolysis test (up to 270 min) was conducted exclusively at 120 °C to simulate realistic field conditions. The titration results are presented in Table 4. For the 30% solid retarded acid solution, the acid concentration reached 3.15 mol/L and 3.50 mol/L after 60 and 120 min of hydrolysis, respectively, comparable to a 15% hydrochloric acid solution. After 270 min, the acid concentration reached 4.06 mol/L. This indicates that at high temperatures, the solid retarded acid reaction does not stop at 120 min; instead, it exhibits the characteristic of rapid acid generation in the early stage and long-term sustained release in the later stage, enabling continuous acid generation and the maintenance of a high acid concentration over an extended period.

Table 4. Sustained acid generation pattern of solid retarded acid at 120 °C.

Temperature (°C)	Time (min)	Group 1 Acid Concentration (mol/L)	Group 2 Acid Concentration (mol/L)	Group 3 Acid Concentration (mol/L)	Mean Acid Concentration (mol/L)
120	0	1.63	1.76	1.62	1.67
	60	3.22	3.06	3.17	3.15
	120	3.42	3.58	3.51	3.50
	180	3.61	3.75	3.74	3.70
	240	3.88	3.83	3.99	3.90
	270	4.01	4.02	4.15	4.06

3.4. Acid Generation Model of Solid Retarded Acid

The mathematical model describing the acid-generation concentration of the solid retarded acid is expressed as follows:

$$C = \frac{B}{B_o}\left[1.67 + \frac{T}{85} erf\left(\frac{t}{25}\right)\right] \quad (1)$$

where, B—Concentration of solid retarded acid, %. B_0—Concentration of solid retarded acid at 30%, %. T—Temperature, °C. t—Time, s. C—Concentration of generated acid, mol/L.

It should be noted that Equation (1) is a semi-empirical regression model based on experimental data. Its fit is less optimal during the first 40 min, reflecting the inherent limitations of empirical modeling. This is primarily because, during the initial stage of the experiment, solid particles undergo a complex non-steady-state process involving heat absorption, softening, and phase-change dissolution. A single regression model struggles to precisely capture the characteristics of this transient phase. However, considering that acid fracturing operations in the ultra-deep wells of the Shunbei Oilfield typically exceed 120 min, the core application goal of solid retarded acid is to achieve effective etching along

the deep fracture length, whereas the near-wellbore zone (0–40 min) is usually dominated by pad fluids or conventional acids. Consequently, this study focuses on acid etching behavior after an acid-rock contact time of 40 min. Experimental data indicate that the model prediction error drops below 5% after 40 min. This demonstrates that the model possesses high reliability for predicting acid concentration in the far-wellbore zone, meeting the engineering requirements for accurate prediction of the effective penetration distance.

To verify the reliability of the model predictions, experimental data from room temperature (25 °C) and 90 °C were selected to fit the solid retarded acid generation model (Equation (1)). This model was then used to predict the acid concentration at 120 °C, and the predictions were compared with the experimental data at 120 °C that were not involved in the fitting process. The fitting results are shown in Table 5.

Table 5. Simulation results of the mathematical model.

Time (min)	25 °C Exp (mol/L)	25 °C Fit (mol/L)	90 °C Exp (mol/L)	90 °C Fit (mol/L)	120 °C Exp (mol/L)	120 °C Fit (mol/L)
0	1.67	1.67	1.67	1.67	1.67	1.67
20	1.56	1.79	2.04	2.32	2.26	2.57
40	1.74	1.83	2.49	2.61	2.77	2.91
60	1.85	1.85	2.76	2.74	3.05	3.03
80	1.85	1.86	2.79	2.8	3.07	3.07
100	1.85	1.86	2.83	2.83	3.08	3.09
120	1.86	1.86	2.85	2.84	3.1	3.1
R^2	0.952		0.968		0.971	
RMSE (mol/L)	0.08		0.14		0.15	
Overall Model Fit	R^2 = 0.964 RMSE = 0.168					

To quantitatively evaluate the fitting quality of the model, the Coefficient of Determination (R^2) and Root Mean Square Error (RMSE) were calculated. The results indicate that the overall model R^2 reached 0.96, and the RMSE was 0.15 mol/L, demonstrating that this empirical model possesses good regression accuracy. These results are presented in Figure 4. The fitted mathematical model exhibited a deviation of approximately 10–15% from the experimental data within the first 0–40 min, with the measured values being slightly lower than the predicted values. However, after 40 min, the model results showed good agreement with the experimental data. The correlation improved with increasing temperature, and at higher temperatures, the model predictions closely matched the measured results. Given that the Shunbei region is characterized by ultra-high formation temperatures (exceeding 120 °C) and prolonged acid–rock contact durations (much greater than 40 min), this model can be employed to predict acid concentration during acid fracture processes in this region. Moreover, the model can be integrated with existing acid-fracturing simulation models to predict the effective acid penetration distance of the solid retarded acid in the fracture.

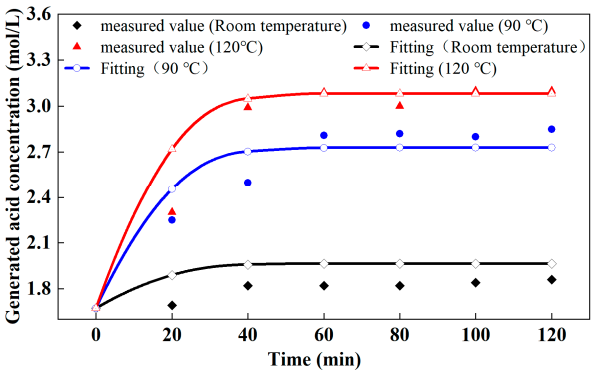


Figure 4. Validation of the acid generation kinetics model: High agreement between model predictions and experimental measurements.

4. The Retardation Performance of Solid Retarded Acid

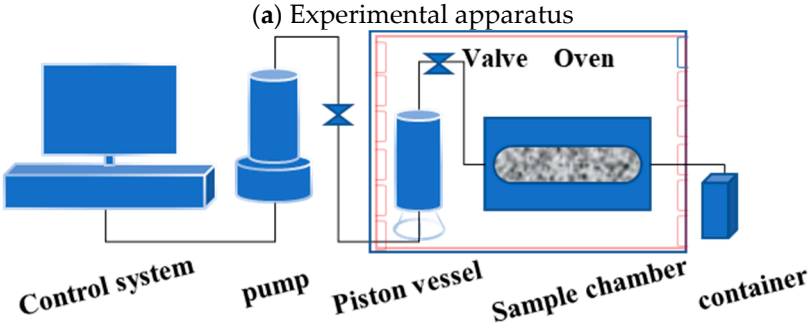
The retardation performance is a key indicator for evaluating the effectiveness of retarded acid systems. It can be assessed by calculating the amount of dissolved carbonate rock when reacted with the solid retarded acid solution. In this method, an excess amount of carbonate rock fragments is reacted with a fixed volume of acid solution. After the reaction, the undissolved carbonate fragments are collected and weighed, and the reaction rate is determined based on the mass difference before and after the reaction. The retardation performance of different acid systems can then be compared according to their reaction rates. This method offers the advantage of simplicity and ease of operation; however, it cannot fully simulate the actual fracture conditions, where the acid simultaneously flows and reacts with the rock. Therefore, in this study, fracture conductivity experiments were employed to simulate the flow and reaction process of solid retarded acid within fractures. The amount of carbonate reacted within a fixed reaction period was used as an indicator to evaluate the retardation performance of the solid retarded acid. In addition, the etched rock plates were subjected to acid-etched fracture conductivity tests to further assess the flow capacity of the acid-etched fractures.

4.1. Experimental Equipment and Methods

The retardation performance evaluation was conducted using a high-temperature and high-pressure acid displacement apparatus manufactured by Jiangsu Hua'an Petroleum Equipment Co., Ltd., Jiangsu China (Figure 5). The experimental setup is shown in Figure 5. The rock used in the experiment was outcrop carbonate samples collected from the Shunbei region, with an average calcium carbonate ($CaCO_3$) content of 93%, permeability of 0.1 mD, and porosity of 8%.



(**a**) Experimental apparatus



(**b**) Schematic diagram of the experimental apparatus

Figure 5. High-temperature acid displacement equipment.

The outcrop samples were cut into rock plates with dimensions of 175 mm × 36 mm × 20 mm using a wire-cutting machine. The plates were immersed in 1% brine for 24 h, then air-dried to remove surface moisture and weighed. Each plate was sealed within the fracture

conductivity cell using a high-temperature and acid-resistant sealant. The fracture aperture between the two plates was maintained at approximately 4 mm to simulate the fracture width during field acid fracturing operations. The conductivity cell was then placed inside the high-temperature acid displacement apparatus. After assembling and connecting the entire system, deionized water was circulated through the system to ensure there were no blockages or leaks. Once normal operation was confirmed, the prepared acid solution with a solid retarded acid concentration of 30% was injected into the piston vessel. The system temperature was increased to 120 °C and preheated for 3 h to ensure both the acid solution and the rock slabs reached the target temperature. After preheating, the displacement pump was activated to perform the acid displacement experiment at a constant injection rate of 50 mL/min. The acid flowed through the artificial fracture formed between the two rock plates, dissolving the rock surfaces. Upon completion of the acid injection, the plates were then removed and weighed again to determine the mass loss caused by acid etching. Considering the difficulty of fully replicating the complex conditions of ultra-deep wells—such as high temperature, high closure stress, large injection rates, and variable fracture widths—in laboratory experiments, this study adopts a research approach combining 'experimental parameter measurement + model prediction.' The experimental section aims to establish a standardized evaluation workflow to accurately determine the intrinsic reaction kinetic parameters and retardation factors of the solid retarded acid under controlled rheological conditions (fixed fracture width and flow rate). Subsequently, the characteristic parameters obtained from experiments are incorporated into the acid fracturing mathematical model established in Section 6, which accounts for variable fracture width and temperature fields. This enables the prediction of the effective acid penetration distance at the field scale of the Shunbei Oilfield.

The amount of the carbonate rock dissolved was measured at acid displacement times of 30, 60, 90, 120, and 150 min. For comparison, two other types of retarded acid systems—cross-linked acid and gelled acid—were tested under identical experimental conditions. The cross-linked acid system consisted of 20% hydrochloric acid, 0.8% SPR-JC gelling agent, and 0.6% SPR-SJL crosslinker, whereas the gelled acid system consisted of 20% hydrochloric acid and 0.8% SPR-JC gelling agent. The hydrochloric acid used in the experiments was analytical grade (Sinopharm Chemical Reagent Co., Ltd., Shanghai China), and both the gelling agent and crosslinker were supplied by Shandong Spring Chemical Co., Ltd., Shandong China. The dissolution performance of the solid retarded acid was compared with that of the cross-linked and gelled acid systems to evaluate its retardation performance. The detailed experimental conditions are summarized in Table 6.

Table 6. Experimental scheme of the retardation performance test.

Experiment Number	Acid Type	Acid-Displacing Time/min
1#	Solid retarded acid	30
2#		60
3#		90
4#		120
5#		150
6#	Cross-linked acid	30
7#		60
8#		90
9#	Gelled acid	30
10#		60
11#		90

Based on the amount of carbonate dissolved, the acid–rock reaction rate per unit area and per unit time was calculated using Equation (2)

$$v = \frac{m}{S \times t} \tag{2}$$

where, v—acid-rock reaction rate, g/(cm^2·min); m—the amount of dissolved rock, g; S—acid-rock contact area, cm^2; t—acid-rock contact time, min. After calculating the reaction rates for different acid types with rock plates, the retardation performance of solid retarded acid can be evaluated using Equation (3) [20]. In Equation (3), γ denotes the retardation rate of the retarded acid; v_0 represents the reaction rate of cross-linking acid and gelled acid, g/(cm^2·min); v_1 denotes the reaction rate of the solid retarded acid, g/(cm^2·min).

$$\gamma = \frac{v_0 - v_1}{v_0} \times 100\% \tag{3}$$

4.2. Experimental Results and Analysis

The rock dissolution amount and reaction rate of the solid retarded acid were measured at acid-rock contact times of 30, 60, 90, 120, and 150 min. Each set was tested in triplicate, and the resulting data are shown in Table 7. The amount of dissolved rock and the reaction rate of the solid retarded acid are presented in Figure 6.

Table 7. Rock dissolution amount and reaction rate under different contact times.

Time (min)	Exp 1 (g)	Exp 2 (g)	Exp 3 (g)	Dissolution Amount (g) Mean	Rate 1	Rate 2	Rate 3	Reaction Rate (g/(cm^2·min)) Mean
30	6.18	6.62	6.40	6.40	1.71	1.83	1.77	1.77
60	11.25	11.97	11.58	11.60	1.55	1.65	1.60	1.60
90	17.20	18.05	17.85	17.70	1.59	1.67	1.65	1.63
120	23.85	25.01	24.34	24.40	1.65	1.73	1.68	1.69
150	26.80	28.10	27.30	27.40	1.48	1.56	1.51	1.52

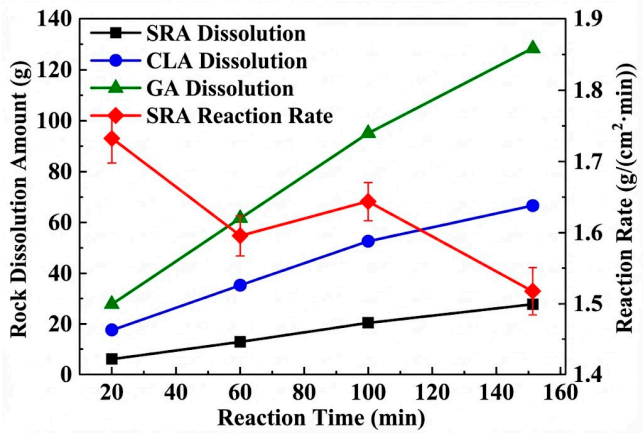


Figure 6. Reaction characteristics of solid retarded acid at 120 °C: Dissolution amount increases linearly with time while consistently maintaining a high reaction rate. (SRA is solid retarded acid; CLA is cross-linked acid; GA is gelled acid).

At a contact time of 30 min, the dissolution amount was 6.4 g. As the reaction time increased, continuous hydrolysis of the solid retarded which generated new H^+ ions, led to a gradual increase in the dissolution amount. After 150 min, the total dissolution reached 27.4 g. Within the first 120 min, the dissolution amount exhibited an approximately linear relationship with reaction time. Given that the carbonate rock plates used in the experiment measured 175 mm × 36 mm × 20 mm, the calculated acid–rock contact area was 60.21 cm^2. The corresponding reaction rates for different reaction times were determined

using Equation (2). Under 120 °C, the solid retarded acid maintained a relatively stable acid–rock reaction rate of approximately 0.0016 g/(cm^2·min) over an extended period, with a high dissolution rate still observed after 150 min. During the 150-min displacement test, the core was maintained in a constant-temperature oven at 120 °C. Since both the injected fluid and the rock system were preheated and kept in an isothermal environment, the temperature was maintained at 120 °C ± 1 °C, and the temperature gradient along the short rock slab was negligible.

Under the same experimental conditions, acid displacement tests were conducted for 30, 60, and 90 min using cross-linked acid and gelled acid systems to compare their dissolution performance with that of the solid retarded acid. The relative retardation rate of the solid retarded acid with respect to the cross-linked and gelled acids was calculated using Equation (3), and the results are summarized in Table 8. At identical temperature and reaction time, the solid retarded acid exhibited a smaller dissolution amount and lower reaction rate compared with both the cross-linked and gelled acids. The relative retardation rate of the solid retarded acid was approximately 60% compared with the cross-linked acid and 78% compared with the gelled acid. These results indicate that the solid retarded acid possesses a superior retardation capability, with an acid–rock reaction rate roughly one-third that of the cross-linked acid and one-fifth that of the gelled acid [21]. This demonstrates that the solid retarded acid is well suited for carbonate reservoirs with rapid acid–rock reaction rates, as it can effectively reduce the reaction rate and extend the acid penetration distance. However, due to its pronounced retardation characteristics, achieving high dissolution amounts and high fracture conductivity requires a longer acid–rock contact time.

Table 8. Comparison of dissolution amount and retardation rate for different acid systems (Mean ± Standard Deviation).

Time (min)	Solid Retarded Acid Dissolution Mass (g)	Cross-Linked Acid Dissolution Mass (g)	Gelled Acid Dissolution Mass (g)	Retardation Rate (vs. Cross-linked Acid (%))	Retardation Rate (vs. Gelled Acid (%))
30	6.40 ± 0.15	18.10 ± 0.18	27.10 ± 0.25	64.6	76.4
60	11.60 ± 0.22	31.70 ± 0.23	58.20 ± 0.36	63.4	80.1
90	17.70 ± 0.23	42.10 ± 0.33	82.50 ± 0.49	58.0	78.5
120	24.40± 0.60	53.5 ± 1.50	105.3 ± 3.00	54.4	76.8
150	27.40 ± 0.65	65.8 ± 1.80	128.4 ± 3.50	58.4	78.7

5. Fracture Conductivity Generated by Solid Retarded Acid

5.1. Experimental Methods

In this study, the fracture conductivity of the acid-etched rock plates under different closure pressures was tested using an FCS2000 fracture conductivity testing system manufactured by CoreLab, Houston, TX, USA (as shown in Figure 7). The two acid-etched rock plates were placed in direct contact within the core holder for the measurement. The test procedures followed the SY/T 6302–2019 standard [22] for fracture conductivity measurement of carbonate plates. In the experiment, each pair of acid-etched rock plates was sealed within the conductivity cell. The inlet and outlet ports of the cell were connected to the pipeline system and differential pressure transducers. The conductivity testing software was used to set the closure pressure from 10 MPa to 90 MPa, increasing in increments of 10 MPa every 60 min. The fluid flow rate was controlled between 5 and 10 mL/min. Before testing, water circulation was conducted through the system to ensure the absence of blockage or leakage. Once normal operation was confirmed, the closure pressure was applied to the rock plates to initiate the test. The flow rate during displacement was monitored using an electronic balance, and the fracture conductivity at each pressure stage was calculated based on the measured flow rate and the pressure difference between the inlet and outlet

of the flow cell. After completing the measurement at a given closure pressure, the system automatically proceeded to the next pressure stage until all pressure conditions were tested.



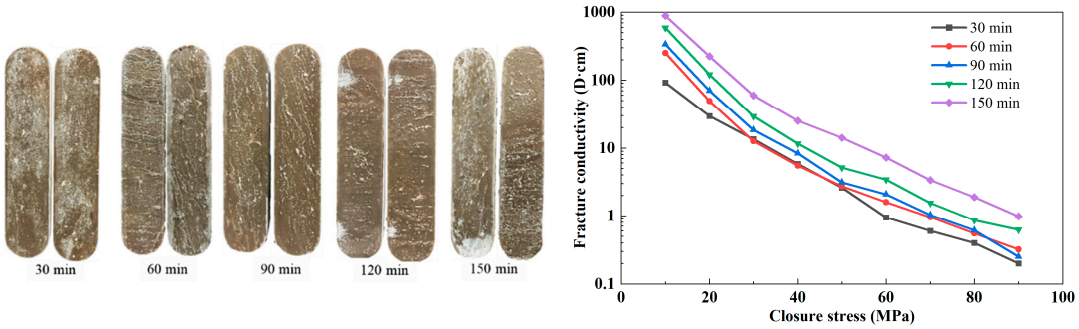
Figure 7. Fracture conductivity test equipment.

5.2. Experimental Results and Analysis

The conductivity of acid-etched fractures is primarily determined by the etching morphology formed after acid–rock interaction [23,24]. The etched fracture morphologies obtained at different acid–rock reaction times are shown in Figure 8a. Observation of the dissolution patterns revealed that the etching depth along the fracture length was relatively uniform, and the overall morphology appeared spotted or banded. This indicates that the acid concentrations at the inlet and outlet of the fracture were similar during the flow process, confirming that the solid retarded acid maintained a good retardation effect under high-temperature conditions. However, noticeable differences were observed with increasing reaction time. As the acid–rock interaction continued, the non-uniformity of the etching pattern became more pronounced, and the height difference between the "peaks" and "grooves" on the fracture surface increased. The acid-etched fracture conductivity was measured under closure stresses ranging from 10 MPa to 90 MPa for reaction times of 30, 60, 90, 120, and 150 min. Each group was tested in triplicate. The calculated average conductivity and standard deviations are presented in Table 9.

This variation in dissolution morphology directly influenced the conductivity of the acid-etched fractures. The conductivity variation with closure pressure and reaction time is illustrated in Figure 8b. As the closure pressure increased, the fracture conductivity decreased. At the same closure pressure, the fracture conductivity increased with greater dissolution extent. For the rock plates etched by the solid retarded acid for 30 min, the initial conductivity was 92.31 D·cm. After 150 min of acidizing, the initial conductivity reached 885.9 D·cm, corresponding to the observed increase in etching heterogeneity. It should be noted that this high value was observed only under a low closure pressure of 10 MPa. This is attributed to the extensive rock dissolution (27.4 g) resulting from the prolonged 150-min reaction, which created open flow channels under low pressure. While deep channels were generated, the effective contact area of the supporting asperities was concurrently reduced. Under high closure stress (>60 MPa), the concentrated stress on these limited support points exceeded the compressive strength of the rock, leading to the crushing and deformation of the supporting asperities. Consequently, the flow channel volume diminished, causing a rapid decline in conductivity. However, the evaluation of acid fracturing effectiveness should prioritize conductivity under high closure pressures. As the closure pressure increased to 60 MPa, the conductivity gradually decreased and stabilized at approximately 5 D·cm. Further analysis of the conductivity curves under different acid–rock times showed that when the reaction time was less than 120 min, the fracture conductivity values were similar at effective closure stresses above 60 MPa.

The acid-etched fracture conductivity remains at approximately 5 D·cm, representing a significant improvement compared to the conductivity observed at reaction times below 120 min. This is because, at 150 min, the non-uniform etching results in rock support points that exceed those at 120 min in both quantity and structural integrity. Consequently, under high closure stress, the connectivity of the fracture etched for 150 min is superior to that of the fracture etched for 120 min, leading to the observed difference in conductivity. Therefore, it is recommended to extend the shut-in period after pumping to allow an acid–rock reaction duration of approximately 3 h, ensuring sufficient dissolution and the formation of high-conductivity etched fractures in the Shunbei carbonate reservoir. To validate the superiority of these results, a comparison was made with the cross-linked acid system commonly used in the field. Based on the dissolution kinetics results in Table 8, the reaction rate of the cross-linked acid is approximately three times that of the solid retarded acid. This demonstrates its technical advantage for the stimulation of ultra-deep reservoirs.



(**a**) Morphology of etched fractures (**b**) Variation curve of fracture conductivity

Figure 8. Influence of reaction time on etching morphology and conductivity patterns: Prolonged reaction improves conductivity under high closure pressure.

Table 9. Acid-etched fracture conductivity under different closure stresses (Mean ± Standard Deviation).

Closure Stress (MPa)	30 min (Mean ± SD)	60 min (Mean ± SD)	90 min (Mean ± SD)	120 min (Mean ± SD)	150 min (Mean ± SD)
10	92.3 ± 4.6	245.1 ± 12.2	345.5 ± 17.3	610.2 ± 30.5	885.9 ± 44.3
20	29.5 ± 1.5	49.6 ± 2.5	71.2 ± 3.6	115.4 ± 5.8	218.6 ± 10.9
30	13.2 ± 0.7	12.4 ± 0.6	18.1 ± 0.9	29.5 ± 1.5	60.3 ± 3.0
40	5.6 ± 0.3	5.8 ± 0.3	8.9 ± 0.4	11.2 ± 0.6	25.1 ± 1.3
50	2.7 ± 0.1	2.5 ± 0.1	3.1 ± 0.2	5.0 ± 0.3	13.6 ± 0.7
60	0.95 ± 0.05	1.54 ± 0.08	2.1 ± 0.1	3.4 ± 0.2	7.2 ± 0.4
70	0.61 ± 0.03	0.95 ± 0.05	1.02 ± 0.05	1.45 ± 0.07	3.4 ± 0.2
80	0.40 ± 0.02	0.61 ± 0.03	0.62 ± 0.03	0.88 ± 0.04	1.85 ± 0.09
90	0.20 ± 0.01	0.32 ± 0.02	0.25 ± 0.01	0.64 ± 0.03	0.98 ± 0.05

6. Acid Concentration Distribution of Solid Retarded Acid Within the Fracture

The previously established temperature field model focused primarily on the temperature distribution within conventional acid fracturing fractures and the influence of temperature on the acid-rock reaction. The acid generation model established in this paper is a function of time, temperature, and acid-generating material concentration. Building upon the previous model, it introduces a mass balance equation for the acid-generating material (Equation (8)), considering the concentration distribution (B) of the solid material. Substituting this into the acid generation model (Equation (1)) yields the acid solution concentration distribution (C). Unlike the temperature field model, the proposed model incorporates an equation describing the concentration variation of the acid-generating material. Rather than being limited to temperature field calculations, it establishes a set of mathematical equations describing the dynamic conversion of solids into acid within the temperature field. By integrating the acid generation model with the acid fracturing model,

it achieves a prediction of the acid concentration distribution, thereby enabling a more accurate prediction of the acid penetration distance. Based on the previously established temperature field model for acid fracturing [25], a solid retarded acid flow–reaction model was developed by integrating the acid-generation model derived in the previous section. The proposed model is established on the principles of mass balance, energy conservation, and acid–rock reaction kinetics, and describes the coupled processes of fracture propagation, acid flow within the fracture, acid–rock reaction, fluid leak off, and temperature distribution. Fracture propagation was represented using the Perkins–Kern–Nordgren (PKN) model [26]. The acid flow within the fracture was characterized by a continuity equation, which governs the temporal and spatial evolution of pressure distribution along the fracture. By solving the continuity equation, the pressure distribution of the acid fluid within the fracture at any given time can be obtained.

$$\frac{\partial bv_x}{\partial x} + \frac{\partial bv_z}{\partial z} + 2v_l = -\frac{\partial b}{\partial t} \tag{4}$$

where x and z denote the coordinates in the fracture length and height directions, respectively, m; b represents the fracture width, m; v_l denotes the acid fluid filtration velocity, m/s; v_x and v_y denote the acid fluid flow velocities in the fracture height and length directions, respectively, m/s, calculated using Darcy's equation:

$$v_x = -\frac{w^2}{12u}\frac{\partial p}{\partial x}, v_z = -\frac{w^2}{12u}\frac{\partial p}{\partial z} \tag{5}$$

Since the acid concentration of the retarded acid is temperature-dependent, it is necessary to determine the temperature distribution within the fracture. The calculation of the temperature field requires consideration of both the temperature distribution in the filtrate zone adjacent to the fracture and that within the acid solution inside the fracture. The coupling between these two temperature fields determines the actual temperature of the acid fluid within the fracture. The energy conservation equation governing the temperature variation of the acid solution flowing inside the fracture is expressed as follows:

$$\rho_{\mathrm{f}} c_{\mathrm{f}} \frac{\partial bT_{\mathrm{f}}}{\partial t} = -\rho_{\mathrm{f}} c_{\mathrm{f}} \left(\frac{\partial bT_{\mathrm{f}} v_x}{\partial x} + \frac{\partial bT_{\mathrm{f}} v_z}{\partial z} \right) + k_{\mathrm{f}} \left(\frac{\partial^2 bT_{\mathrm{f}}}{\partial x^2} + \frac{\partial^2 bT_{\mathrm{f}}}{\partial z^2} \right) + 2\frac{k_{\mathrm{f}} N_{\mathrm{u}}}{w} (T_{\mathrm{d}} - T_{\mathrm{f}}) - 2\rho_{\mathrm{f}} c_{\mathrm{f}} v_{\mathrm{l}} T_{\mathrm{f}} \tag{6}$$

In the equation, ρ_f denotes the density of the acid solution, kg/m^3; c_f denotes the specific heat capacity of the acid solution, J/(kg·°C); k_f denotes the thermal conductivity coefficient of the acid solution, W/(m·°C); N_u denotes the Nusselt number; T_f denotes the temperature of the acid solution, °C; T_d denotes the temperature of the diffusion filtrate zone, °C. The energy conservation equation within the filtrate zone is:

$$\xi \left[c_f \rho_f \phi + c_r \rho_r (1-\phi) \right] \frac{\partial T_d}{\partial t} = c_f \rho_f v_l \left(T_f - T_d \right) + \frac{k_f Nu}{b} \left(T_f - T_d \right) + K_{ef} (T_{res} - T_d) \frac{1}{\sqrt{\pi D \tau}} \frac{e^{-\frac{F^2}{D}}}{1 + erf\left(\frac{F}{\sqrt{D}} \right)} \tag{7}$$

where: c_r denotes the specific heat capacity of the formation rock, J/(kg·°C); ρ_r denotes the density of the formation rock, kg/m^3; ϕ is the matrix porosity; and ξ is the thickness of the diffusion-filtrate zone, m. k_d is the heat transfer coefficient of the diffusion-filtrate zone, obtained from equation $K_{\mathrm{d}} = \frac{k_{\mathrm{f}} Nu}{w}$; K_{ef} is the thermal conductivity coefficient of the rock outside the diffusion-filtrate zone, determined by equation $K_{ef} = \phi k_f + (1-\phi) k_r$ (where Kr is the formation thermal conductivity coefficient), W/(m·°C); T_{res} denotes the original formation temperature, °C. D and F are defined as below. C_t represents the total rock compressibility coefficient.

$$F = \frac{c_f \rho_f C_t}{c_f \rho_f \phi + c_r \rho_r (1-\phi)} \cdot D = \frac{K_{ef}}{c_f \rho_f \phi + c_r \rho_r (1-\phi)} \tag{8}$$

The key distinction between the proposed model and conventional acid flow–reaction models lies in the inclusion of the mass balance equation for the solid retarded acid (Equation (9)). In this equation, the first two terms on the left-hand side represent the variation in the concentration of the solid retarded acid within a given fracture caused by convective transport over a unit time. The middle terms account for the change in concentration due to hydrolysis, while the final term represents the acid-generating material lost to the formation through leakoff. The right-hand side of the equation denotes the accumulation term. By solving this equation, the concentration distribution of the solid retarded acid within the fracture at each time step can be obtained, expressed as $B(C, x, z, t, T)$.

$$-\frac{\partial(Bv_x b)}{\partial x} - \frac{\partial(Bv_z b)}{\partial z} - \frac{\partial(B(C,x,z,T_f,t)v_x b)}{\partial x} - \frac{\partial(B(C,x,z,T_f,t)v_z b)}{\partial z} - 2v_l B = \frac{\partial(Bb)}{\partial t} \tag{9}$$

Substituting the concentration profile of the solid retarded acid into the acid generation model of solid retarded acid yields the acid solution concentration distribution $C(x, z, B, T, t)$ within the fracture. Furthermore, this enables the derivation of the acid solution concentration equilibrium Equation (10), which accounts for both the simultaneous reaction and hydrolysis characteristics of the solid retarded acid.

$$-\frac{\partial(Cv_x b)}{\partial x} - \frac{\partial(Cv_z b)}{\partial z} + \frac{\partial(C(x,z,B,T_f,t)v_x b)}{\partial x} + \frac{\partial(C(x,z,B,T_f,t)v_z b)}{\partial z} - 2(v_l + k_g)C = \frac{\partial(Cb)}{\partial t} \tag{10}$$

By applying the fracture width increment Equation (11), the etched fracture width distribution generated by solid retarded acid can be obtained for each time step.

$$(2k_g C + 2\eta v_l C)\frac{\beta}{\rho_r(1-\phi)} = \frac{\partial b}{\partial t} \tag{11}$$

Herein, k_g denotes the hydrogen ion mass transfer coefficient, m/s; v_l denotes the leak-off velocity; η represents the proportion of the two components in the filtrate acid solution participating in wall etching, typically approaching zero, and is taken as zero in this paper; β denotes the acid solution dissolution capacity, kg/kg; other symbols retain their meanings as above.

Based on the model, simulations were conducted with an injection rate of 6 m^3/min and an acid-generating material concentration of 30%, while other formation parameters were adopted from reference [25] are listed in Table 10 and Table 11, respectively.

The simulated acid concentration distributions of the solid retarded acid within the fracture at injection times of 20, 40, 60, and 80 min are shown in Figure 9, and Figure 10 presents the variation of acid concentration along the fracture centerline for injection times ranging from 80 to 160 min. The acid-generation behavior of the solid retarded acid was jointly controlled by time, temperature, and solid retarded acid concentration. At the early stage of the fracturing (10–20 min), due to the short injection time and high fracture temperature, the generated acid was rapidly consumed, resulting in a relatively low initial acid concentration and a rapid decline thereafter. When the injection time reached 40 min, the temperature within the fracture decreased, and the fracture width increased, leading to a reduction in flow resistance. As a result, the newly generated acid could propagate farther toward the fracture tip. Meanwhile, significant cooling near the wellbore caused a lower acid concentration at the fracture entrance, producing a non-monotonic concentration profile along the fracture centerline that first increased and then decreased. Throughout the dynamic fracture length, the generated acid concentration of the solid retarded acid

remained above 2%, indicating that the effective acidizing region extended across the entire dynamic fracture. This demonstrates that the solid retarded acid can substantially enhance the effective acid penetration distance. Under typical field operating conditions (a pumping duration of approximately 2 h), the effective acidizing distance can reach more than 150 m.

Table 10. Treatment parameters and stratigraphic parameters for Shunbei well #T [25].

Parameters (Units)	Value	Parameters (Units)	Value
Reservoir depth (m)	6500	Geothermal gradients (°C/m)	0.0226
Reservoir temperature (°C)	145.2	Porosity (%)	0.2
Fracture height (m)	50	Temperature of injected fluid (°C)	25
Injection rate (m^3/min)	6	Young's modulus of the rock (MPa)	36,700
Poisson ratio	0.26	Thermal conductivity of the rock (W/m·K)	5.2
Density of the rock (kg/m^3)	2700	Specific heat capacity of the reservoir crude oil (J/kg·K)	1981
Specific heat capacity of the reservoir rock (J/kg·K)	999	Thermal conductivity of crude oil (W/(m·K))	0.339
Density of crude oil (kg/m^3)	840	-	-

Table 11. Injection parameters for Shunbei well #T [25].

Parameters (Units)	Value	Parameters (Units)	Value
Density (kg/m^3)	1090–1110	Specific heat capacity (J/kg·K)	4180
Coefficient of thermal conductivity (W/(m·K))	0.65	Acid concentration (%)	15
Acid–rock reaction rate constant (mol/cm^3)	0.9849×10^{-6}	The heat generated by the acid–rock reaction (kJ/mol)	$\Delta H_m^{\Theta}(T, p)$
Order of the reaction (dimensionless)	0.88	Mass transfer coefficient (m/s)	1.4693×10^{-5}

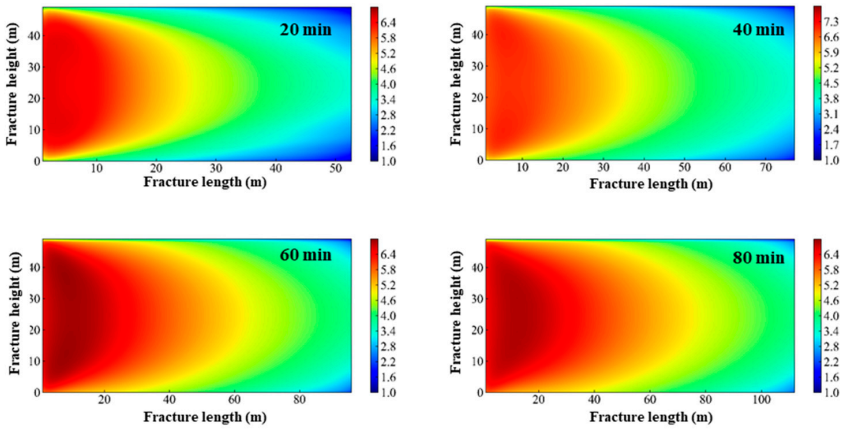


Figure 9. Simulation results of the acid concentration field within the fracture: The concentration of solid retarded acid in the deep fracture increases with injection time.

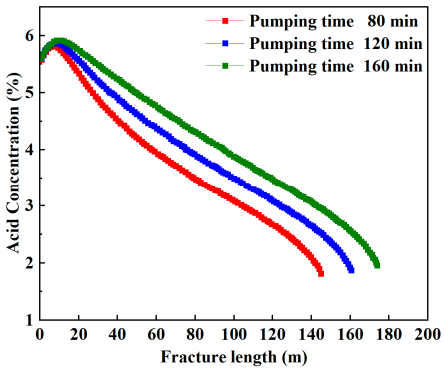


Figure 10. Acid generation concentration curves of solid retarded acid: Effective acid penetration distance exceeds 150 m under typical operating conditions.

7. Conclusions

A series of experimental evaluations was conducted to investigate the comprehensive performance of the solid retarded acid system. The main conclusions are summarized as follows:

(1) Solubility of the acid-generating material was strongly influenced by both temperature and solid retarded acid concentration. When the solid retarded acid concentration was below 20%, complete dissolution occurred at room temperature. However, at concentrations above 20%, complete dissolution could not be achieved at room temperature. When the concentration was 30%, the solid retarded acid was fully dissolved after 40 min at 120 °C.

(2) Temperature had a significant impact on the generated acid concentration. At room temperature, the increase in acid concentration was limited, whereas under high-temperature conditions, the acid concentration exceeded 3.5 mol/L, which is comparable to that of a 13% hydrochloric acid. Compared with conventional acids, the solid retarded acid exhibited superior retardation performance, with an overall reaction rate approximately one-third that of cross-linked acid and one-fifth that of gelled acid.

(3) The fracture conductivity of the solid retarded acid remained above 5 D·cm under an effective closure stress of 60 MPa after 150 min of acid–rock reaction. Therefore, it is recommended to extend the shut-in period after pumping to allow an acid–rock reaction duration of approximately 3 h to ensure effective etching and sustained fracture conductivity.

(4) The developed acid-generation model is a function of time, temperature, and acid-generating material concentration, and can be used to predict the acid concentration during acid fracturing. When coupled with an acid fracturing mathematical model, it can effectively predict the acid penetration distance. Simulation results predicted based on the experimentally derived kinetics model indicate that, under typical operating conditions in the Shunbei Oilfield (120 min reaction time), the effective penetration distance of the solid retarded acid can exceed 150 m. This confirms the material's potential for deep penetration.

Author Contributions: Conceptualization, J.M. and K.C.; formal analysis, J.C.; funding acquisition, K.C.; methodology, J.M. and B.G.; project administration, L.Z.; resources, J.M. and L.Z.; supervision, J.M. and L.Z.; writing—original draft, X.L. and Y.Z.; writing—review and editing, B.G. All authors have read and agreed to the published version of the manuscript.

Funding: This research was funded by the Key Laboratory of Marine Oil & Gas Reservoirs Production, Sinopec, grant number: 33550000-22-ZC0613-0311.

Data Availability Statement: The original contributions presented in this study are included in the article. Further inquiries can be directed to the corresponding author.

Conflicts of Interest: Authors Jia Cui, Kai Chen, and Lufeng Zhang were employed by the Sinopec, Petroleum Exploration and Production Research Institute. The remaining authors declare that the research was conducted in the absence of any commercial or financial relationships that could be construed as a potential conflict of interest.

References

1. Xu, Z.; Dai, C.; Zhao, M. Research and application progress of crosslinked gelled acid. *Appl. Chem. Ind.* **2017**, *46*, 2424–2427.
2. Wang, Y.; Li, Y.; Cheng, X. New acid fracturing technique for carbonate reservoirs with high-temperature and deep layer. *Acta Petrolei Sinica.* **2012**, *33*, 166–173.
3. Yeager, V.; Shuchart, C. *In Situ Gels Improve Formation Acidizing*; PennWell Corporation: Tulsa, OK, USA, 1997; Volume 95, pp. 70–72.
4. Mou, J.; Zhang, S. Influence factor analysis on acid pressure rips diversion capacity. *Pet. Geol. Recovery Effic.* **2011**, *18*, 69–71+79+115.

5. Chen, Z.; Dai, Y. Current status and future prospects of acid fracture technology for deep carbonate reservoirs. *Pet. Drill. Tech.* **2005**, *1*, 58–62.
6. Liu, W.; Xiong, N.; Wu, Z. Review on types of retarded acid and application of emulsified acid. *Adv. Fine Petrochem.* **2010**, *11*, 12–15.
7. Cui, B.; Feng, P.; Yao, E. Etching geometry and conductivity of acid-etched fractures injected with retarded acid slug: Taking low-porosity and low-permeability carbonate reservoir of F Oilfield in Iraq as an example. *Pet. Geol. Oilfield Dev. Daqing* **2023**, *42*, 74–80.
8. Xu, Z.; Qi, N.; Zhang, Z.; Han, Z.; Su, X. Development and evaluation of authigenic acid system in high-temperature carbonate reservoirs. *Appl. Chem. Ind.* **2021**, *50*, 2344–2347. [CrossRef]
9. Mu, D.; Jia, W.; Yao, Y.; Yang, C.; Wang, C.; Jia, J. Study on the integration of gelled acid and crosslinked acid to form high temperature retarded acid. *Drill. Fluid Complet. Fluid* **2019**, *36*, 634–638.
10. Zhang, H.; Chen, M. Study and application of organic retarded acid in eastern peripheral oilfields in Daqing. *Pet. Geol. Oilfield Dev. Daqing* **2006**, *25*, 57–58.
11. Yuan, L.; Xiong, Y.; Jiang, Y.; Zhang, Q. Development and evaluation of high temperature emulsified acid. *Chem. Eng. Oil Gas* **2014**, *43*, 521–524.
12. Nasr-El-Din, H.; Al-Dahlan, M.; As-Sadlan, A.; Al-Zamil, H.A. Iron precipitation during acid treatments using hf-based acids: Proceedings. In Proceedings of the SPE International Symposium on Formation Damage Control, Lafayette, LA, USA, 20–21 February 2002.
13. Zhou, G.; Xu, B. Self-Generating Acid, Its Preparation Method and Use. CN102899012B, 2 March 2016.
14. Song, Z.; Duan, Y.; He, S.; Wang, X.; Li, W.; Chen, Y.; Xu, G.; Liu, H. Combination of acid fracturing fluid system for ultra-deep carbonate reservoir in fuman oilfield and its application. *Drill. Prod. Technol.* **2023**, *46*, 139–145.
15. Lu, Y.; Qi, N.; Zhou, S.; Wang, Z.; Li, X.; Su, X.; Wang, L. Acid-etching fracturing law of multi-stage alternating injection in limestone reservoirs. *Pet. Geol. Recovery Effic.* **2024**, *31*, 119–127.
16. Taylor, K.; Nasr-el-din, H. Laboratory evaluation of in-situ gelled acids for carbonate reservoirs. *SPE J.* **2003**, *8*, 426–434. [CrossRef]
17. Wei, X.; Wang, Y.; Zheng, S. Current study on acid applying to carbonate reservoir. *West-China Explor. Eng.* **2008**, *148*, 63–65.
18. Luo, J.; Cao, C.; Hu, W. Self-generating acid system suitable for Tahe oilfield. *Petrochem. Ind. Technol.* **2015**, *22*, 199–207.
19. Li, Y.; An, N.; Fang, Y.; Luo, P.; Yu, W.; Meng, X. Study on preparation and properties of long-term high temperature resistant autogenic acid. *Chem. Res. Appl.* **2021**, *9*, 1834–1837.
20. Liu, F.; Zhang, S.; Cao, N. Study and evaluation of highly permeable retarded acids. *Drill. Fluid Complet. Fluid* **2022**, *39*, 365–372.
21. Liu, C.; Gou, B.; Guan, C. Effect of well shut-in on acid etching morphology and conductivity. *J. China Univ. Pet. (Ed. Nat. Sci.)* **2021**, *45*, 96–103.
22. National Energy Administration. *SY/T 6302–2019: Procedures for Measuring the Conductivity of Proppants*; Petroleum Industry Press: Beijing, China, 2019.
23. Zhang, T.; Zhou, H.; Zhang, L.; Zhao, Y.; Huang, S.; Zhang, M.; Zhu, L.; Zhang, R. Pore-scale investigation of bottom water invasion dynamics in carbonate gas reservoirs with different interlayer distributions. *Nat. Gas Ind. B* **2024**, *11*, 140–153. [CrossRef]
24. Che, M.; Yang, Z.; Tian, Z.; Yang, L.; Zhang, L. Research on acid liquid delay. In Proceedings of the 2016 China Oil and Gas Field Development Chemicals Symposium, Beijing, China, 20–21 July 2016.
25. Mou, J.; He, J.; Zheng, H.; Zhang, R.; Zhang, L.; Gao, B. A new model of temperature field accounting for acid–rock reaction in acid fracturing in Shunbei oilfield. *Processes* **2023**, *11*, 294. [CrossRef]
26. Zhang, Q. *Principles and Design of Oil Production Engineering*; Petroleum University Press: Dongying, China, 2006.

Disclaimer/Publisher's Note: The statements, opinions and data contained in all publications are solely those of the individual author(s) and contributor(s) and not of MDPI and/or the editor(s). MDPI and/or the editor(s) disclaim responsibility for any injury to people or property resulting from any ideas, methods, instructions or products referred to in the content.